A Multipurpose Optical MEMS Sensor for Harsh Environments

P. Nieva[*], N. McGruer[**] and G. Adams[***]

[*]Department of Mechanical Engineering, University of Waterloo
200 University Ave. W., Waterloo, ON, N2L 3G1, Canada, pnieva@uwaterloo.ca
Northeastern University, Boston, MA, USA, [**]mcgruer@ece.neu.edu, [***]adams_g@coe.neu.edu

ABSTRACT

This paper presents a new multifunctional MEMS sensor for the simultaneous measurement of displacement, pressure and temperature. The sensor is based on a Fabry-Perot Micro-Opto-Mechanical Device (FPMOD) which is completely passive and consists of a micromachined optical cavity formed between a Silicon substrate and a top Silicon Nitride film in the form of a cantilever beam. When affixed to a vibrating surface, the amplitude and frequency of vibration are determined by illuminating the device with a monochromatic light source and analyzing the back reflected light to determine deflection of the beam with respect to the substrate. The effect of air viscous damping in the out-of-plane motion of the FPMOD is used to simulate its operation as a pressure-temperature sensor. The small size of the sensor, the materials in which it can be built, and its simple construction make it suitable for on-chip integration and ideal for harsh high-temperature applications.

Keywords: Harsh environments sensors, optical MEMS, multifunctional MEMS sensor, pressure-temperature sensor

1 INTRODUCTION

MEMS sensors for harsh environments are critical in many application fields and essential for reducing weight and volume in strategic market sectors such as automotive, aerospace, turbomachinery, oil-well/logging, nuclear power and communications [1, 2]. Placing microsensors closer to the ultimate point of use will reduce weight, decrease complexity, and improve machine reliability [1]. The integration of various elements into a sensor module is important for enhancing their performance. Integration allows for multiple quantities to be measured with one chip, increasing reliability, and facilitating installation. For example, MEMS sensor systems that simultaneously measure steady and transient phenomena (e.g., temperature, pressure, vibration and flow parameters) in or near the hot-gas path are needed to maximize the efficiency of turbine engines or more generally, combustion engines [2].

An economical way to deal with higher temperatures and other aggressive environmental conditions is to build the sensors out of robust materials [1, 2]. These materials should exhibit high thermal, chemical and mechanical stability and, for economic reasons, should facilitate easy integration with standard Silicon micromachining [1-3]. For example, high-temperature MEMS sensors have been developed using Si as the substrate material and LPCVD Silicon Nitride [3] or SiC [4, 5] as the sensing material. Their thermal, mechanical, and optical properties permit the fabrication of optical microstructures that, when combined to optical interferometric techniques, allow the design of non-contact MEMS sensor systems [6-9] suitable for localized precision measurements in harsh environments at temperatures up to 600°C (which is the point at which the mechanical properties of Si start to deteriorate,[2]).
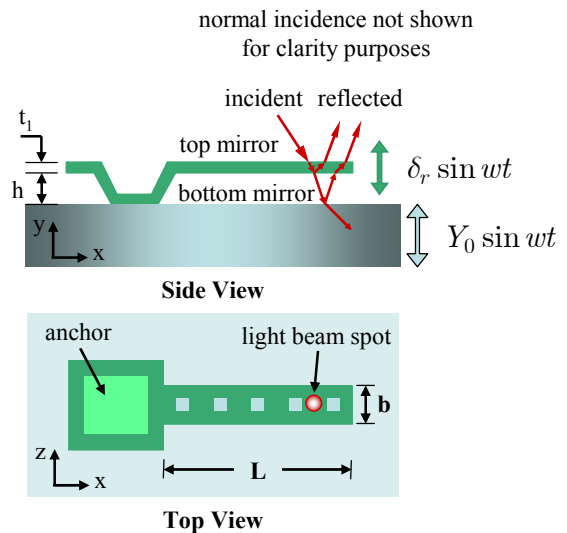

Figure 1: Schematic diagram of the FPMOD cantilever beams studied in this work.

In this paper, we report on an optical MEMS sensor based on a micromachined Fabry-Perot structure [8, 9] that is suitable for high temperature applications. The basic schematic of the sensor (Fig. 1) uses a cantilever beam fabricated in low-stress Silicon-rich LPCVD Nitride (Si_xN_y) as the top mirror and the silicon substrate below as the bottom mirror of the Fabry-Perot structure. These two mirrors form an optical microcavity for a monochromatic laser beam incident at the top. For this arrangement, the total interferometric light back-reflected from the FPMOD depends on the height of the optical microcavity or air gap, h. When the substrate vibrates with a harmonic motion $Y_0 \sin wt$ (Y_0 and ω are the amplitude and frequency

respectively), there is a relative deflection of the cantilever beam with respect to the substrate $\delta_r \sin wt$ and hence a change in the microcavity height. The amplitude of the substrate motion can be calculated by measuring the back-reflected light.
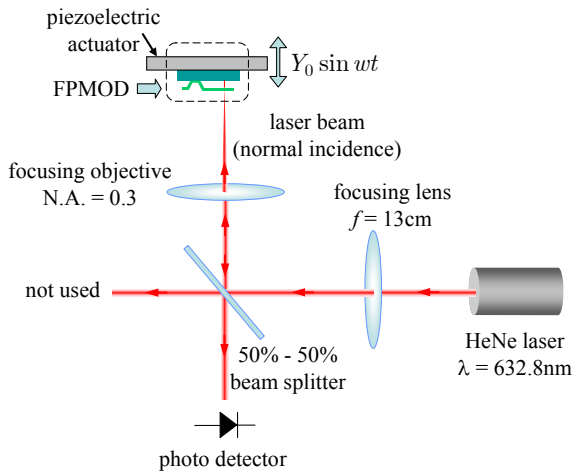

Figure 2: Schematic of the optical setup for the measurement of the interferometric back reflected light.
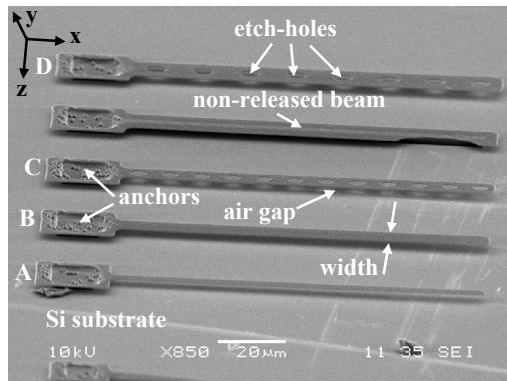

Figure 3: SEM micrograph of a set of released FPMOD cantilever beams, 120µm nominal length.

Beam Type	Length (µm)	Width (µm)	Etch-Hole diameter (µm)	Air Gap @ spot (µm)	Spot Location (µm)
A	122.5	4.25	-	2.84	5
B	119.6	8.17	-	2.66	17.5
C	123.5	9.31	3.92	2.60	17.5
D	118.5	13.39	5.56	2.62	22.5

Table 1: Summary of measured parameters for FPMOD cantilever beams included in this paper

The optical setup for the measurement of the back reflected light is shown schematically in Fig. 2. This approach has the advantage of compatibility and ease of integration with well-developed silicon micromachining technologies. In addition, the flexibility in response range and sensitivity achieved by adequately designing the shape

and size of the mirrors and the air gap height [9] permits the fabrication of similar FPMOD structures with different sensing capabilities on the same chip.

2 DESIGN AND OPERATION

Figure 3 shows a SEM (Scanning Electron Microscope) micrograph of FPMOD cantilever beams fabricated using the 2-mask process described in [8, 9]. Table 1 lists the relevant dimensions including the location on the FPMOD surface at which the incident light is directed (measured along the length of the beam and starting from the tip).

The FPMOD is designed to detect the vibration of the substrate in the y-axis (see Fig. 1). As shown in Fig. 2, the interferometric back-reflected light is obtained by directing the light beam of a JDS-Uniphase 1122/P He-Ne laser (wavelength $\lambda = 632.8$ nm) to the FPMOD mounted on a piezoelectric actuator (EDO EC-97). This actuator provides a small harmonic displacement excitation to the substrate of the surface-bonded test chip (4mm x 4mm in size) at a certain frequency. A focusing lens, a beam splitter, and a focusing microscope objective are used to focus the laser beam down to a 15µm spot at a normal incidence and direct the back-reflected interferometric signal of the vibrating FPMOD to a photo detector operated in the biased mode. The electrical current generated by the photo detector is processed to determine the relative deflection of the top mirror with respect to the position of the bottom mirror at the frequency of excitation. The experimental FPMOD frequency response (see Fig. 5) is determined by repeating this sequence for different frequencies in the range of interest (between 2 and 200 kHz). The mechanical characteristics of the device and the measured frequency response provide the means to predict the behavior of the FPMOD, i.e. the relationship of the measured optical interferometric signal to the vibration of the substrate.

2.1 Optical Interferometric Signal

The optical microcavity of the FPMOD corresponds to a Fabry-Perot in reflectance. Thus, its optical response is given by the *power reflectance*, R, of the top of its surface. In other words, the optical signal detected by the photodiode during sensor operation. Assuming no variation in the top mirror thickness or the relaxed cavity height, R is only a function of the Nitride layer thickness t_1, and the time-dependant air cavity height at the location of the laser beam spot, i.e. $t_2 = h + \delta_r \sin(wt)$ [10].

Figure 4 shows the dependence of R on the air gap height (dotted curve). This function was obtained from the optical signal measured from the FPMOD type A vibrating at a frequency of 62kHz and fitted to the AC component of the theoretical power reflectance model [10] with h, δ_r, and t_1 as the fitting parameters. The function is periodic (period $\lambda/2$) and represents the optical transfer function of the microcavity of the FPMOD sensor. In this case, the fitting procedure indicated that the static air gap height was

$h = 2.86\mu m$ with a beam thickness of $t_1 = 0.447\mu m$ and a relative displacement amplitude of $\delta_r = 143.8nm$. The total displacement of the beam with respect to the substrate is indicated by the solid line. The values of h and t_1 are within ~3.3% and ~1.5%, respectively, of the measured values listed in Table 1. The static air gap height at the location of the laser beam spot defines the operation point of the sensor which in this case is very close to the point of maximum slope or maximum sensitivity of the transfer function. Motions as small as tenths of nanometers can be resolved using this optical system which is comparable to the resolution reported in [6] for a similar optical interferometric technique.
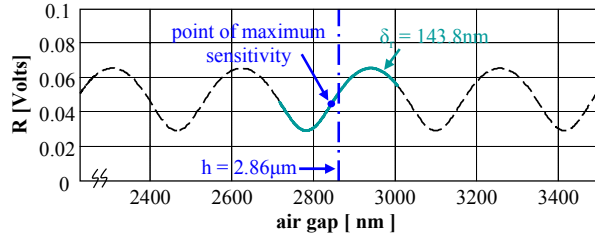

Figure 4: Reflectance of the FPMOD type A as a function of air gap height.

2.2 Mechanical Modeling

For a small amplitude vibration, the FPMOD cantilever beam is considered a continuous system undergoing a harmonic excitation due to substrate motion. If $y(x,t)$ denotes the absolute displacement of the beam, its net displacement with respect to the substrate is $\delta_r(x,t) = y(x,t) - Y_0 \sin(\omega t)$. Neglecting beam thickness variation and beam curvature, the dynamic equation of motion using the *Euler-Bernoulli beam theory* is [8]

$$\frac{\partial^2}{\partial x^2}\left[EI\frac{\partial^2\delta_r}{\partial x^2}\right] + \rho A\frac{\partial^2\delta_r}{\partial t^2} = \rho A Y_0 \omega^2 \sin wt + f(x,t) \quad (1)$$

where ρ is the mass density of the Si_xN_y beam (2865 kg/m³), E is the Si_xN_y Young's modulus (238 GPa [9]), $I = bt_1^3/12$ is the moment of inertia of the cantilever beam cross-sectional area ($A = bt_1$). In (1), $\rho A Y_0 \omega^2 \sin(\omega t)$ represents the effective excitation force per unit length and $f(x,t)$ corresponds to the force per unit length acting on the beam owing to the *air viscous damping* [8, 9]

$$f(x,t) = -(c_s(x) + c_a)\frac{\partial\delta_r}{\partial t}$$

$$c_s = \mu\left(\frac{b}{h}\right)^3\left[\left(1 - \frac{d_1}{d}\right) + \frac{1}{4}\left(1 - \frac{d_1}{b}\right)^3\frac{d_1}{d}\right]\left[\frac{1}{1 + \varepsilon\left(\frac{x}{L}\right)^2}\right]^3$$

$$c_a = \frac{3}{2}\pi\alpha(\mu + b\sqrt{\rho\mu\omega}) \quad (2)$$

In (2), $c_s(x)$ is the coefficient of squeeze film damping resulting from the damping force in the narrow gap, c_a is the coefficient of airflow damping resulting from the damping force in the free space; d_1, d, and ε are parameters related to the etch-hole size and the initial curvature of the beam; ρ (1.3 kg/m³) and μ (1.8 x 10⁻⁵ N.s/m²) are the density and viscosity of the air respectively; and $\alpha \approx 5.5$ was determined experimentally in [9].

2.3 Experimental Results

The solution to (1) provides the necessary insight to the FPMOD bending sensitivity to the harmonic oscillation of the substrate as a function of the structure's geometry. From this solution, the non-dimensional *total viscous damping factor*, ζ_n, and the fundamental resonant frequency f_1 are given by [8, 9]

$$\zeta_n = \frac{I_n + c_a}{2\rho A\omega_n}, n = 1,2,\ldots \quad (3)$$

$$\omega_1 = 2\pi f_1 = (1.8751)^2\sqrt{\frac{EI}{\rho A L^4}} \quad (4)$$

where I_n is the dissipation term due to squeeze film damping. The results shown in Figure 6 are for the FPMOD cantilever beams included in Table 1 to which a 10nm amplitude harmonic excitation has been applied. The devices were tested at atmospheric pressure (1 atm) and room temperature (23°C). By fitting the measured data shown in Fig. 6 to the solution of (1) with the modal resonant frequencies f_n (n=1,2) and total viscous damping factors ζ_n as fitting parameters, their experimental values can be determined. The average fundamental frequency for all these cantilever beams is 43.5 ± 3 kHz.
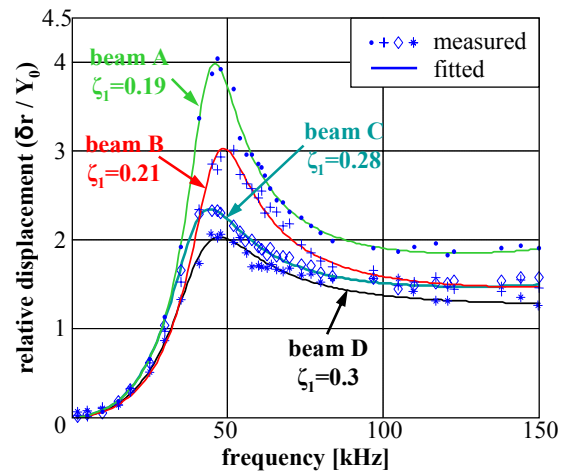

Figure 5: Measured and fitted frequency response for all FPMOD cantilever beams listed in Table 1

The performance of the FPMOD depends strongly on the total air viscous damping [8, 9]. Although squeeze-film

damping is generally believed to be the dominant source of dissipation in oscillating microbeams [5, 6], the agreement between the calculated and measured data suggests that both squeeze-film damping and airflow damping are significant sources of dissipation for these structures. Results show that the effect of the airflow damping becomes relatively more important as the air gap increases. This is attributed to the fact that the squeeze-film damping decreases as the cube of the air gap and the airflow force depends strongly on the properties of the air surrounding the beam and the frequency of excitation.

3 MULTIPLE SENSING

The dependence of the mechanical performance of the FPMOD on the total air viscous damping can be used to design a microsensor capable of detecting pressure and temperature at the same time [9] by using two FPMOD cantilever beams that have different frequency response.
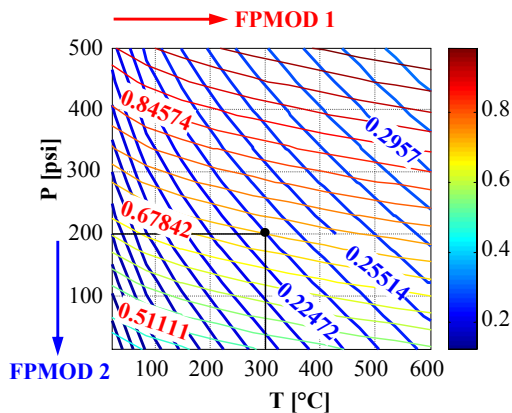

Figure 6: Multifunctional FPMOD operation. At 200°C and 300psi, ζ_1=0.71 for FPMOD 1, and ζ_1=0.23 for FPMOD 2

Consider, for example, two beams of the same length ($L = 120\mu m$), no initial curling and no etch holes. For convenience, the thickness ($t_1 = 0.54\mu m$), and air gap heights are selected for maximum optical sensitivity [9]. The air gap height for the first beam (FPMOD 1) is 1.55µm and for the second beam (FPMOD 2) is 3.45µm. If the air is assumed to be dry [9] and their total viscous damping factors ζ_1 (mode 1), are calculated as a function of pressure and temperature using (3), we obtain the contour plots shown in Fig. 6. The quasi-horizontal contours correspond to FPMOD 1, the quasi-vertical ones correspond to FPMOD 2, and the points at which they intersect are unique. The shift in sensor displacement $\Delta\delta_r$ due to a shift of temperature ΔT and/or pressure ΔP is given by [9]

$$\Delta\delta_r = \left.\frac{d\delta_r}{dP}\right|_T \Delta P + \left.\frac{d\delta_r}{dT}\right|_P \Delta T \qquad (5)$$

The minimum detectable shift in pressure and/or temperature can be found by setting $\Delta\delta_r$ of both sensors

equal to their minimum detectable displacement [9]. Provided that both devices are driven at their fundamental resonant frequency (51.9 kHz) and a known excitation amplitude, shifts on the order of $\Delta T = 13.5°C$ and $\Delta P = 19psi$ can be detected for temperatures and pressures around 350ºC and 284 psi respectively. To further explore the sensitivity of these devices, the effects of humidity on the density of the air, and the effect that pressure, temperature, and air composition may have on the indices of refraction are being investigated.

4 CONCLUSIONS

We have reported on the optical and mechanical characterization of an optical MEMS sensor that can be used for the simultaneous measure of pressure, temperature and vibration. The measured frequency response of the FPMOD cantilever beams shows extremely good agreement with the theory. The major effect that the viscosity and the density of the air have on the damping provides the mechanism for the detection of temperature and pressure changes. We have shown that if two adequately designed FPMOD cantilever beams are driven at their fundamental resonant frequency and at a known displacement excitation it is possible to measure pressure and temperature in harsh high-temperature environments. Since there is no pressure load across the FPMOD cantilever beams, these sensors will not exhibit creep when cycled from high to low pressure. In addition, since the air is trapped by the viscous damping effects there is no need for a sealed cavity. Finally, the very simple configuration in this optical interferometric system will be considered in the future for the integration in the sensor package.

REFERENCES

[1] M. R. Werner and W. R. Fahrner, IEEE Trans. Industrial Electronics, 48(2), 249-257, 2001.

[2] M. Mehregany, C. A. Zorman, N. Rajan, and C. H. Wu, Proc. IEEE, 86(8), 1594-1610, 1998.

[3] P. Nieva, P. Zavracky, G. Adams, H. Tada, A. Abramson, I. Miaoulis and P. Wong, Proc. 5th ASME/JSME Joint Thermal Eng. Conf., 1999.

[4] M. Fonseca, J. English, M. von Arx, and M. Allen, J. Microelectromech. Syst., 11(4), 337-343, 2002.

[5] R. Wiser, M. Tabib-Azar, M. Mehregany and C. Zorman, J. Microelectromech. Syst., 14(3), 579-589, 2005.

[6] T. Stievater, W. Rabinovich, H. Newman, J. Ebel, R. Mahon, D. McGee, and P. Goetz, J. Microelectromech. Syst., 12(1), 109-116, 2003.

[7] R. Waters and M. Aklufi, Applied Physics Letters, 81(18), 3320-3322, 2002.

[8] P. Nieva, PhD Thesis, Dep. Elect. & Comp. Engineering, Northeastern University, 2004.

[9] P. Nieva, N. McGruer and G. Adams, Smart Structures and Materials, Proc. SPIE, San Diego, California, 2006.